

SEREP: Semantic Facial Expression Representation for Robust In-the-Wild Capture and Retargeting

Arthur Josi^{1*} Luiz Gustavo Hafemann^{2*} Abdallah Dib² Emeline Got² Rafael M. O. Cruz¹
Marc-André Carbonneau²

¹Ecole de Technologie Supérieure ²Ubisoft LaForge



Figure 1. SEREP captures facial expressions in challenging in-the-wild conditions, including extreme expressions and side views. These are effectively retargeted to a new head geometry preserving the target identity.

Abstract

Monocular facial performance capture in-the-wild is challenging due to varied capture conditions, face shapes, and expressions. Most current methods rely on linear 3D Morphable Models, which represent facial expressions independently of identity at the vertex displacement level. We propose SEREP (Semantic Expression Representation), a model that disentangles expression from identity at the semantic level. It first learns an expression representation from unpaired 3D facial expressions using a cycle consistency loss. Then we train a model to predict expression from monocular images using a novel semi-supervised scheme that relies on domain adaptation. In addition, we introduce MultiREX, a benchmark addressing the lack of evaluation resources for the expression capture task. Our experiments show that SEREP outperforms state-of-the-art methods, capturing challenging expressions and transferring them to novel identities. Project page is available on the following [link](#).

*Equal contribution

1. Introduction

3D facial performance capture is essential for applications ranging from virtual communication to video games, where users interact with avatars that can be rendered from different viewpoints. While established technologies such as light stages [12] and head-mounted cameras allow for high-fidelity facial capture, they are costly and impractical for general end-users. This motivates research on capturing 3D facial expressions in natural, unconstrained environments using everyday devices like webcams and smartphones.

Capturing 3D facial performance can be viewed as two subtasks: (i) face geometry reconstruction to uncover identity (i.e., face at a neutral expression) and (ii) time-dependent geometry deformation capture to describe facial expressions. Representing these two types of information in disentangled spaces allows for 3D facial reenactment, often called animation retargeting, by applying the acting performance to a character with a different morphology. This implies that facial expressions are represented at a semantic level instead of direct vertex displacements which are cou-

pled with the geometry of a given identity. In addition to allowing for reenactment, disentangled representations can improve performance on downstream tasks [6,35,36] while reducing sample complexity [2,42]. In this paper, we focus on learning a meaningful facial expression representation, assuming that we already have access to a neutral face geometry.

Most models for in-the-wild face expression capture [10, 11, 13, 17, 20, 39, 45] rely on 3D Morphable Models (3DMM) [28, 33] to represent a facial mesh through independent identity and expression bases. In these models, expressions are represented as additive vertex displacements to a neutral mesh. In reality, a semantic facial expression (e.g., wide smile) cannot be simply represented by vertex displacements that can readily be applied to any identity. Mesh deformations inherent to an expression directly depend on the underlying face morphology (i.e., identity). For instance, a smiling expression results in different displacements on two persons, depending on their facial traits, such as the shape of the mouth or the fat tissue structure. This indicates that disentanglement of expression and identity must happen at the semantic level instead of the vertex level as formulated in 3DMMs.

In addition to not truly capturing the semantics of expression, 3DMM-based methods struggle to capture accurate 3D face meshes. While they show promising results when viewed from the original camera angle, issues appear in novel views. This is particularly noticeable in images where the subject does not directly face the camera. In these cases, viewing the 3D reconstruction from other angles reveals artifacts such as asymmetric mouth shapes and distorted expressions. These issues are explained by the self-supervised training strategy which optimizes models using differentiable rendering [29] without explicit 3D supervision. While this approach allows for training on large-scale in-the-wild data, it primarily enforces consistency in the original camera space but produces geometric inconsistencies that are only revealed when changing viewpoints. Some methods [46, 47] circumvent these issues by training exclusively on realistic synthetic data, however modeling and rendering realistic variations in skin, eyes, hair, clothing, and accessories requires significant effort and expertise.

Another key challenge in advancing in-the-wild face capture is the lack of standardized evaluation protocols to measure geometric accuracy. Current evaluation protocols rely on qualitative visual comparisons and on projecting geometry into camera view to use image-space metrics like similarity measures [27], emotion recognition [10, 39] or alignment of face segmentation masks [1, 40]. This reprojection step introduces inaccuracies in measurement and does not allow for evaluating the whole face geometry due to limited points of view. While benchmarks like NOW [41] and REALY [7] exist for evaluating the 3D geometry of

neutral expressions, there is no public benchmark for assessing the geometric accuracy of captured facial animations.

In this paper, we propose a method for monocular 3D face capture named *SEREP*, that addresses the fundamental challenges described above. We introduce a semantic face expression basis, learned from unpaired 3D poses, without supervision in the form of expression, FACS, or emotion labels. We validate the expressivity of our semantic expression representation by measuring the reconstruction error from ground truth expressive 3D meshes and measure how identity is preserved when transferring expression between identities. Our results indicate better identity preservation compared to traditional 3DMM methods.

To address the lack of standardized evaluation protocols measuring geometric accuracy in 3D space, we introduce MultiREX, a new benchmark based on the Multiface dataset [51]. MultiREX contains challenging expressions, different viewpoints of the same subject, and high-quality ground truth geometry, allowing for meaningful reconstruction accuracy evaluation. We show that *SEREP* is more accurate for 3D performance capture than competing methods and more robust to viewpoints than recent state-of-the-art methods.

Finally, we present visual results for in-the-wild capture and retargeting, which demonstrate improved results on challenging expressions. Overall, our method improves the state-of-the-art in terms of identity preservation after expression transfer, and the geometric reconstruction of expressions from monocular images, especially on non-frontal views. Our contributions are summed up as follows:

- We introduce an identity-aware expression representation that encodes the semantics of facial expression.
- We propose a semi-supervised training strategy that combines synthetic and in-the-wild data through domain adaptation.
- We create and publicly release MultiREX, the first video-based geometric facial expression reconstruction benchmark. We see this contribution as an important step towards the advancement of research on face geometry reconstruction from monocular images and videos.

2. Related work

3D Morphable Models. Facial performance capture from monocular video is an ill-posed problem, as the task is to recover 3D geometry from a 2D projection of the face in the image. To make this problem tractable, most recent methods [8, 10, 11, 17, 20, 31, 45, 58], rely on statistical morphable models (3DMM) [16], such as [8, 28, 32, 33] to constrain

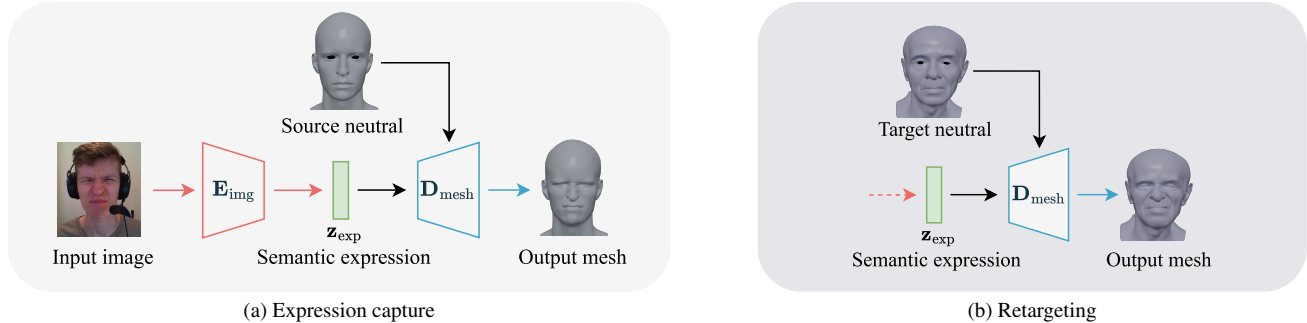


Figure 2. Overview of the expression capture and retargeting processes. Given an input image, we extract a semantic expression code \mathbf{z}_{exp} using the encoder \mathbf{E}_{img} . **Left:** The decoder \mathbf{D}_{mesh} applies this code to the neutral mesh to obtain the expressive 3D mesh. **Right:** In a retargeting scenario, the same semantic expression code is used with a target neutral mesh of any other subject.

the problem. These morphable models use a large collection of scans and define: (i) a template mesh \mathbf{T} (average face shape), (ii) an *identity* (shape) basis \mathbf{S} , and (iii) an *expression* basis \mathbf{E} . An arbitrary mesh M is then defined by identity (β) and expression coefficients (ψ) of these linear bases: $M = \mathbf{T} + \beta\mathbf{S} + \psi\mathbf{E}$. We note that a given expression vector ψ results in the same vertex displacement regardless of the identity and, therefore, cannot capture the *semantic meaning* of an expression. In other words, the same semantic expression of two subjects would have different displacements and, therefore, different expression codes.

Semantic expression disentanglement. Some recent work proposed approaches for semantic expression disentanglement. Facescape [53] considers a corpus of multiple identities performing the same set of expressions, and represents identity and expression with a bilinear model for identity and expression [44]. Neural Parametric Head Models [23] also uses a corpus of multiple identities performing the same expressions. This model operates in an implicit representation, where expression deformations are represented with an MLP that takes both expression and identity coefficients as input. We note that both methods require paired data for training (multiple subjects performing the same expression). This has two drawbacks: (i) it is costly to acquire, (ii) for a given expression label, they assume that the subjects are performing exactly the same facial movements. In reality, subjects are not always capable of following the exact instructions for these poses. Other works [9, 54] require facial animations to be decomposed in FACS-based rigs, a task that normally requires a significant amount of manual work. In contrast, we learn a semantic expression space with unpaired data, without any labels or rig decomposition, in a more similar vein to the work done in face reenactment [15, 52].

In-the-wild face capture. Most recent methods for in-the-wild face capture train models in a large collection of in-the-wild images, in a self-supervised manner [10, 11, 14, 17, 20, 45, 58]. These methods estimate the identity and expression parameters of a 3DMM, as well as camera, light, and reflectance information of a scene, then use a differentiable renderer [29, 43] to render a synthetic image of the parametrized scene. The model is trained to minimize the difference between rendered images and ground truth, together with auxiliary losses. Since these losses are only based on camera-space information, we observe that these methods can sometimes produce implausible expressions when viewed from other angles, notably when the processed subject is not facing the camera.

Another research direction shows that training models on photo-realistic synthetic data can generalize to in-the-wild capture [25, 46, 48]. These methods render large datasets of synthetic images by controlling: identity, expression, texture, hair, clothes, and accessories. They use a large collection of artist-made and procedurally generated assets to reduce the gap between synthetic and real data.

In this work, we introduce a mixed training procedure, using real and synthetic data. Rather than attempting to close the synthetic-to-real domain gap through complex 3D modeling, we use a simple procedure to obtain synthetic data and bridge the domain gap with a domain adaptation strategy.

Performance evaluation. Most existing work on monocular face reconstruction provides either (i) qualitative results, (ii) quantitative results on image-centric metrics, or (iii) geometric error in reconstructing neutral meshes. Image-centric metrics include emotion classification [10, 39], and the Intersection-Over-Union of segmented face regions in the predicted mesh, compared to a pseudo-ground truth [1, 45]. Geometric reconstruction error is commonly computed using either the NOW [41] and REALY [7] benchmarks, which only provide data in a neutral

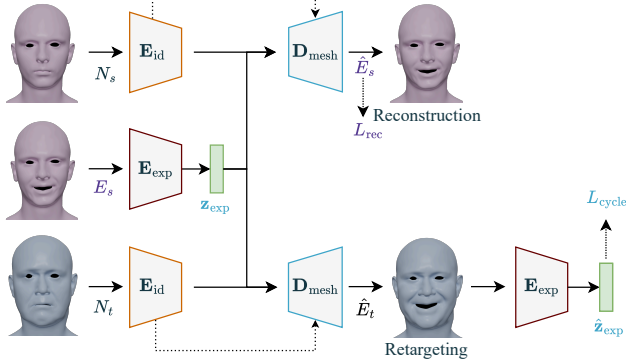


Figure 3. Expression retargeting model. The model learns to reconstruct a source expression E_s given the source neutral N_s or to retarget it to a target neutral N_t . The cycle loss aligns the codes \mathbf{z}_{exp} for the same semantic expressions of different subjects.

pose, being unsuitable for evaluating expression recovery. FaceWarehouse [5] allows for assessing expression capture in static 3D meshes, but provides low-quality scans from RGBD data and does not include multiview capture.

In this work, we propose a new public benchmark for geometric expression capture based on the Multiface [51] dataset. This dataset was collected from a light stage with multiple cameras and provides higher-quality reconstructions. Our proposed benchmark allows for geometric evaluation of expression capture from monocular videos under controlled camera angles.

3. Method

We propose a two-stage training to capture facial expressions from in-the-wild images and videos. In the first stage, we train a semantic face expression model (Sec. 3.1) that disentangles expression from identity in 3D facial meshes. In the second stage, we train a facial performance capture model (Sec. 3.3) to predict expression codes from monocular images. The final 3D mesh is produced by combining the expression code with a neutral mesh, as illustrated in Fig. 2. The target neutral mesh can be estimated using methods such as [14, 58], and is outside of the scope of this work.

3.1. Semantic face expression model

We train the semantic face expression model on a retargeting task as illustrated in Fig. 3. Training samples consist of a neutral mesh N_s , an expressive mesh E_s from the same source subject, and a neutral mesh N_t from a target subject. The task of the model is to (i) reconstruct the ground truth expression E_s , and (ii) retarget the expression to the target subject.

This model is composed of an encoder \mathbf{E}_{id} that encodes identity, an encoder \mathbf{E}_{exp} that encodes expression, and a sin-

gle decoder \mathbf{D}_{mesh} that decodes the final mesh. All models operate directly on mesh vertices, using spiral convolutions [4]. Both encoders consist of 5 blocks containing a spiral convolution followed by a graph pooling operation [37]. The last layer is a fully-connected layer, that produces the identity and expression codes. The decoder consists of a fully-connected layer followed by 5 blocks of graph upsampling and spiral convolutions. We use skip connections between intermediate features of the identity encoder and the mesh decoder. We describe the loss terms used in training below.

Reconstruction loss. We use the squared L_2 distance between vertices of the source expressive mesh E_s and its reconstruction \hat{E}_s : $L_{\text{rec}} = \|\hat{E}_s - E_s\|^2$.

Cycle consistency loss. The model should represent the same semantic expressions for different subjects with the same expression code. Without paired expression data, there is no ground truth for the retargeted mesh. Thus, we use a cycle consistency loss [55] to encourage semantic expressions to remain the same after retargeting on the target identity: $L_{\text{cycle}} = \|\mathbf{z}_{\text{exp}} - \mathbf{E}_{\text{exp}}(\hat{E}_t)\|^2$.

Edge preservation loss. We use edge length regularization L_{edge} , similar to [3], to reduce jagged edges on the decoded meshes. This loss penalizes large changes in edge length between the retargeted mesh \hat{E}_t and the neutral N_t .

Eye closure loss. This term, noted L_{eyes} enforces eye closure. We compute the distance between the two polylines defined by the sequence of vertices of the upper and the lower eyelid. This term is enforced when the source expression E_s contains a closed eye.

Delta loss. We complement our data set of expressive meshes with an additional set of neutral meshes to improve generalization to new identities. These additional target neutral meshes N_t require a supplementary loss term to stabilize the training. This term, defined as $L_{\text{delta}} = \|(\hat{E}_t - N_t) - (E_s - N_s)\|^2$ prevents the decoder from collapsing to a trivial solution and producing neutral meshes regardless of the expression code.

The complete training loss for the retargeting model \mathcal{L}_{ret} is consequently defined as follows:

$$\mathcal{L}_{\text{ret}} = L_{\text{rec}} + L_{\text{cycle}} + L_{\text{delta}} + L_{\text{edge}} + L_{\text{eyes}} \quad (1)$$

Importance weights are omitted for better readability and detailed in supplementary material.

3.2. Synthetic data generation

Once the semantic face expression model is trained, we exploit it to generate a synthetic dataset that will be used to train the face expression capture model. First, we sample a target identity N_t and expression code \mathbf{z}_{exp} from the dataset and produce an expressive mesh \hat{E}_t . We procedurally place a set of teeth and eyes, and a random face albedo

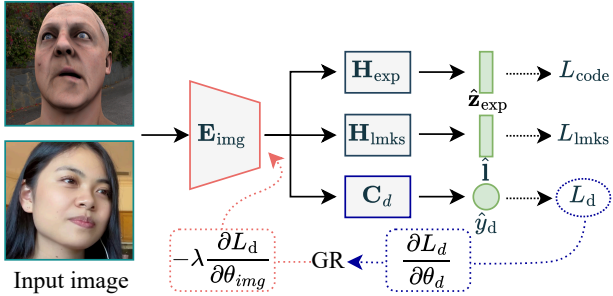


Figure 4. Face expression capture. Given a synthetic or real input image, the model estimates the expression code \mathbf{z}_{exp} , landmarks \mathbf{l} , and the domain (real or synthetic). Gradient reversal (GR) and the classifier \mathbf{C}_d are used to bring real and synthetic images close in feature space.

texture, environment map, and head pose. Finally, we render a synthetic image using [21]. Unlike [46], we do not add accessories, hair, or clothes to the scene, avoiding any further 3D modeling. Examples of the generated images can be visualized in the supplementary material. We also extract 2D facial landmarks, denoted \mathbf{l} , by projecting the corresponding mesh vertices to camera coordinates.

3.3. Face expression capture model

Our face expression capture model estimates a semantic expression code given an image, as illustrated in Fig. 4. The model is jointly trained on three tasks enabling joint training on synthetic and real data. The encoder \mathbf{E}_{img} extracts latent features ϕ from the image. From these shared features, the head \mathbf{H}_{exp} estimates the expression code $\hat{\mathbf{z}}_{\text{exp}}$, and the head \mathbf{H}_{lmks} estimates the 2D landmarks $\hat{\mathbf{l}}$. A classifier \mathbf{C}_d predicts whether the sample is a real or synthetic image for domain adaptation.

The encoder \mathbf{E}_{img} uses a ConvNeXt-B backbone [34]. The \mathbf{H}_{code} head and the domain classifier \mathbf{C}_d each consists of 3 blocks of linear layers and group normalization [50], with skip-connections [24]. The \mathbf{H}_{lmks} head is a single linear layer. The low capacity of the \mathbf{H}_{lmks} head encourages the encoder to produce features ϕ that encode the necessary information for landmark prediction, the task shared between both domains.

Our training loss comprises three terms:

Latent code loss. This term encourages an accurate prediction of the expression code, but can only be applied to synthetic samples since we do not have ground truth expression data for in-the-wild images. It is defined as $L_{\text{code}} = \|\hat{\mathbf{z}}_{\text{exp}} - \mathbf{z}_{\text{exp}}\|^2$.

Landmarks loss. This term is the pixel distance between the predicted landmarks and the GT landmarks defined as: $L_{\text{lmks}} = \|\hat{\mathbf{l}} - \mathbf{l}\|^2$. Landmark prediction is the shared task between both domains; therefore, the loss term applies to

all images, real and synthetic. It ensures that the features ϕ encode information about salient regions of the face regardless of the image domain.

Domain loss. To minimize the domain gap between synthetic and real data, we adopt the domain adaptation approach from [22]. The classifier \mathbf{C}_d is trained to distinguish between real and synthetic images. During gradient descent optimization, we reverse the sign of the gradient after \mathbf{C}_d and scale its magnitude by a factor λ . As a result, \mathbf{C}_d is optimized to discriminate between the two domains, while the features ϕ are encouraged to discard domain-specific information, thus aligning the distributions of both domains more closely.

The training loss for this model is defined as follows:

$$\mathcal{L}_{\text{cap}} = L_{\text{code}} + L_{\text{lmks}} + L_{\text{domain}} \quad (2)$$

In summary, the model learns to encode images into a semantic expression code \mathbf{z}_{exp} , using the ground truth codes from the synthetic data. The landmark and domain loss terms align the features from real and synthetic images allowing the model to generalize to in-the-wild images. Importance weights in Eq. (2) are omitted for clarity and detailed in the supplementary material.

4. Experiments on expression representation

The experiments in this section evaluate the semantic face expression model (Sec. 3.1). We detail its implementation and assess its performance on reconstructing expressions and preserving identity in retargeting.

4.1. Implementation detail

We train the expression model using two datasets: static neutral meshes, and expressive sequences. We use neutral scans from 865 individuals, and dynamic sequences from 10 subjects, each captured over sessions lasting 3 to 19 minutes. These sequences cover a variety of expressions and talking sequences. We evaluate our results on static scans of 56 subjects, including a neutral mesh and 19 expressions. All meshes share the same topology, with 13k vertices.

We jointly train the encoders \mathbf{E}_{id} , \mathbf{E}_{exp} , and the mesh decoder \mathbf{D}_{mesh} , to minimize Eq. (1) using the Adam optimizer [30]. Training on a single A4000 GPU took 3 days.

In all experiments, we use the official implementation of each baseline taken from their respective code repository. For quantitative experiments, results reported in bold are statistically significant based on a Wilcoxon signed rank test ($\rho < 0.001$).

4.2. Expression reconstruction

First, we evaluate the ability of the proposed method to reconstruct expressive face meshes from 56 identities from

the test set. For each expressive mesh, we define an optimization problem: given the subject’s neutral and expressive meshes, find the expression coefficients that minimize the reconstruction loss. We compare our method to the widely used FLAME model [33], evaluating all 1064 expressive meshes from the test set.

In Tab. 1, we report the mean reconstruction error, averaging over all meshes, and considering only a frontal mask of the face. Our method outperforms FLAME, indicating that our expression model is better able to capture the geometric deformations caused by expressions on unseen subjects. We hypothesize this improvement stems in part because it is a non-linear model, which is often more expressive than their linear counterparts. Interestingly, the generalization capability does not come at the price of larger training corpus given that our model was trained using neutral meshes from 865 subjects and animated meshes from 10 subjects, while the FLAME model was trained using 3800 neutral subjects and animations from 24 subjects.

4.3. Identity preservation

We now evaluate the identity preservation of the models on an expression retargeting task. For this evaluation, we consider all pairs of [source, target] subjects from the test set. For each expressive mesh, we obtain the optimal expression code (as in Sec. 4.2) and apply it to the target’s neutral mesh. In total, we obtain 61,600 retargeted meshes for each method. We render the retargeted meshes using the GT neutral texture and a 50mm camera using Blender. Finally, we measure the similarity between the rendered images of the GT and the retargeted images using the cosine similarity (CSIM) of identity embedding as commonly done in face re-enactment research [15,26,38]. A higher CSIM indicates a better preservation of the identity. In other words, a lower source identity traits leakage on the retargeted mesh.

Tab. 1 reports the result of this experiment. As a lower bound, we also report the mean CSIM between random subjects with the same expression. Our method produces retargeted meshes that better preserve the identity of the target person when compared to FLAME. This confirms that the identity and expression bases from FLAME do not allow for fully capturing the semantics behind a given expression and that identity leakage occurs. In contrast, our semantic expression model is better able to retarget an expression preserving the target person’s identity.

Method	Rec. Error (↓)	CSIM (↑)
Random	-	0.501 ± 0.11
FLAME	1.36 ± 0.34	0.766 ± 0.08
Ours	1.15 ± 0.24	0.791 ± 0.08

Table 1. Mean reconstruction error in mm and cosine identity similarity (CSIM) of retargeted expressions against ground truth.

5. Experiments on capture and retargeting

In this section, we evaluate the performance of SEREP (Sec. 3.3) on two applications: expression capture and retargeting. We first introduce MultiREX, our proposed open-source benchmark, which enables comparison of geometric expression capture.

5.1. MultiREX Benchmark

MultiREX (Multiface Region-based Expression evaluation) is based on the Multiface dataset [51]. It evaluates the estimated geometry of monocular face capture systems considering complex expression sequences under multiple camera views. In particular, the protocol evaluates mesh deformations related to expression alone, treating the identity as a given.

The benchmark includes 8 identities captured simultaneously from five viewpoints: *Frontal*, two *Angled* views (yaw rotation around 40 degrees), and two *Profile* views (yaw rotation around 60 degrees). Each subject performs a range-of-motion sequence covering a wide range of expressions, including extreme and asymmetrical motions. The benchmark comprises 10k ground truth meshes and 49k images.

We obtain the ground truth identity (i.e., neutral mesh) by manually selecting a neutral frame for each subject and retopologizing the corresponding mesh to the FLAME topology using commercial software. From these two meshes, we compute a per-subject sparse conversion matrix that enables fast conversion from the FLAME to the Multiface topology.

Inspired by the REALY benchmark [7], we adopt a region-based evaluation method, dividing the face into four regions and performing region-based rigid alignment before assessment. This avoids penalizing a model due to rigid misalignment between the predicted and GT meshes, and instead focuses on the non-rigid deformations. The regions we evaluate are the forehead, cheek, mouth, and nose. For each region, we find the optimal rigid alignment between the GT and predicted meshes in the Multiface topology and compute the per-vertex error. Masks and alignment details are provided in the supplementary material.

We publicly release¹: (i) the code to download assets, (ii) neutral meshes in the FLAME topology alongside the code to convert between FLAME and Multiface topologies, (iii) code to run the benchmark and compute the metrics.

5.2. Implementation details of the capture model

We train the face expression capture model using in-the-wild and synthetic images. For in-the-wild data, we use WFLW [49], which contains 10k face images annotated with landmarks. We complement with CelebV-HQ [57] from which we sample four frames per video and apply

¹Link to code and assets - Coming soon

Method	Cheek	Forehead	Mouth	Nose	Average
DECA [18]	3.54 ± 1.59	1.82 ± 0.70	3.71 ± 1.81	1.30 ± 0.47	2.59
EMICA [11]	3.26 ± 1.57	1.65 ± 0.72	3.44 ± 1.86	1.10 ± 0.47	2.36
SMIRK [39]	4.13 ± 1.59	1.84 ± 0.66	3.69 ± 1.47	1.29 ± 0.43	2.74
Ours (synth only)	2.89 ± 1.38	2.13 ± 0.78	3.05 ± 1.67	1.11 ± 0.44	2.30
Ours	2.83 ± 1.28	1.89 ± 0.81	2.95 ± 1.51	1.08 ± 0.45	2.19

Table 2. Expression reconstruction results on MultiREX. We show per-vertex average errors (in mm) on different facial regions.

an off-the-shelf landmark detector [56] to obtain pseudo ground truth. This amounts to 165k images.

In addition, we generate 135k synthetic images following the procedure described in Sec. 3.2. We project mesh vertices to camera coordinates to obtain ground truth landmarks in image space, except for eyebrows. Recent work [19] notes that eyebrow landmarks are not precise when obtained from mesh vertices of synthetic data. The location of eyebrows in a synthetic image depends on both mesh and texture information. In our work, we simply obtain eyebrow landmarks using a landmark detector [56].

During training, we minimize Eq. (2) using the Adam optimizer [30]. We apply standard data augmentations such as translations, rotations, scale, and occlusions with random patches. Training took 11 hours on two A4000 GPUs.

5.3. Results on MultiREX

We now show quantitative results on geometric expression capture, on the proposed MultiREX benchmark. In all tables, results reported in bold are statistically significant based on a Wilcoxon signed rank test ($\rho < 0.001$). We process videos from all subjects and camera views, comparing our model to DECA [18], EMICA [10,11] and SMIRK [39]. For this experiment, we use ground truth bounding boxes, computed from projecting keypoint vertices to the image space.

For all models, we consider that the neutral mesh is given, therefore only accounting for geometric deformations due to the facial expressions. For a given source image X , with identity mesh N_s , we obtain the expressive mesh $M = \mathbf{D}_{\text{mesh}}(\mathbf{E}_{\text{exp}}(X), \mathbf{E}_{\text{id}}(N_s))$. For the other methods, we use their image encoders to obtain the expression coefficients Ψ , and apply them directly to the neutral mesh $M = N_t + \Psi \mathbf{E}$. For the FLAME-based models, this is followed by the Linear Blend Skinning (LBS) function for jaw rotation.

Tab. 2 reports the average reconstruction error in millimeters for different regions of the face and the average over all face regions. Our method outperforms other state-of-the-art methods on average and on all individual regions except for the forehead region. These improvements over competing methods are explained by the expressivity of our representation and the robustness of SEREP to viewpoints.

Method	Frontal	Angled	Profile
DECA [18]	2.57 ± 1.58	2.61 ± 1.66	2.61 ± 1.70
EMICA [11]	2.17 ± 1.40	2.30 ± 1.55	2.49 ± 1.77
SMIRK [39]	2.25 ± 1.25	2.58 ± 1.61	3.11 ± 1.80
Ours	2.08 ± 1.19	2.08 ± 1.29	2.30 ± 1.40

Table 3. MultiREX expression reconstruction results on frontal and side views.



Figure 5. Facial expression capture examples on MultiREX. Left: Ground truth (GT) mesh of the target subject. Right: predictions for different models on each camera view.

We further analyze the viewpoint robustness of each method by reporting the average reconstruction errors for each viewing angle independently in Tab. 3. These results indicate that our model maintains performance better than competing methods as the viewing angle shifts from the frontal view. In contrast, the performance of EMICA and SMIRK decreases faster as the camera angle increases. This can be visualized in Fig. 5, where we show results

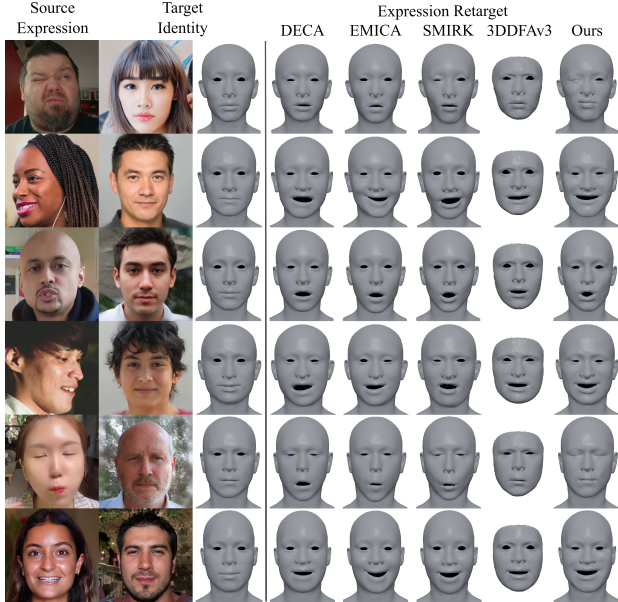


Figure 6. In-the-wild expression retargeting results. Expressions estimated on the source image are applied to a target identity.

for the same expression reconstructed from five different views. Additional examples are provided in the supplementary material. Our model produces consistent results across views, particularly in side views when compared to competing methods. This is especially apparent in the mouth shape of the subject. This is explained by the fact that our method relies on a semantic space that represents facial expressions in their entirety, rather than relying solely on image space information where some regions may be occluded.

5.4. In-the-wild retargeting results

In this section, we compare our method with recent state-of-the-art techniques, DECA [17], EMICA [11], SMIRK [39], and 3DDFA-V3 [45], on the expression retargeting task from in-the-wild images. Since ground truth data for corresponding expressions across subjects on in-the-wild images is not possible to obtain, we compare methods qualitatively. We show several examples in Fig. 6, where the expressions from the images on the first column are transferred to the target identities of the second one.

This is done similarly to the procedure in Sec. 5.3, but here we consider a neutral mesh from another subject, N_t , obtained with an off-the-shelf reconstruction method [14]. 3DDFAv3 uses the Basel 3DMM, which does not use LBS for jaw movements, so this step is not applied.

As can be observed in these examples², SEREP reproduces challenging asymmetrical expressions better than the other methods. For instance, it completely shuts the eyes and closes the mouth on lines 1 and 5. On line 3, SEREP

²More examples in the supplementary material

produces a funnel mouth. On the side views of the second and fourth lines, SEREP produces more plausible facial expressions than other methods, which corroborate the results of Sec. 5.3. This illustrates the benefits of representing expressions at the semantic level instead of in terms of vertex displacements. A wink, a crooked smile, and a mouth pucker semantically mean the same for everyone and do not depend on viewpoint. Lastly, while our model is trained on individual frames, we obtain time-consistent results applying it to videos. The supplementary video showcases this result for both MultiREX and in-the-wild videos.

6. Limitations

We focus on facial expression capture and consequently assume a known identity. We acknowledge that the methods used for comparison in our experiments, while being the best candidates to our knowledge, were designed to address the broader task of reconstructing facial shape, expression and textures.

In addition, our benchmark currently only supports the FLAME topology. Although FLAME is the most widely used 3DMM, extending the benchmark to include other topologies such as Basel [28], ICT [32], and HiFace [8], would facilitate the comparison of a broader range of methods. Finally, our method struggles with external occluders such as glasses and inflated cheeks given that they are not represented enough in the training data.

7. Conclusion

In this work, we present SEREP, a 3D facial expression capture model that operates at a semantic level, enabling precise capture and retargeting of in-the-wild facial expressions. We introduce a semi-supervised learning framework in which we first train a semantic expression encoder using unpaired data, subsequently used to guide the training of our expression capture model. This capture model leverages ground truth expression codes used to generate synthetic image data, as well as facial landmarks from both synthetic and in-the-wild images, to enhance accuracy.

Our experiments underscore the strengths of our expression representation, demonstrating its effectiveness for precise expression capture and retargeting from in-the-wild images. We show that SEREP handles complex expressions and remains robust across various capture conditions, including diverse viewpoints. Additionally, we introduce MultiREX, a new benchmark that evaluates expression capture directly in 3D space, eliminating the measurement imprecision caused by projecting geometry back into image space, as done in previous evaluation protocols. For future work, we aim to make our capture model temporally aware to improve video capture quality and plan to integrate camera position information for enhanced supervision.

8. Acknowledgements

We would like to thank authors of the Multiface dataset [51], as well as authors of DECA [18], EMICA [11], SMIRK [39], and 3DDFAv3 [45] for releasing their code and advancing research in the field.

References

- [1] Kelian Baert, Shrishya Bharadwaj, Fabien Castan, Benoit Maujean, Marc Christie, Victoria Abrevaya, and Adnane Boukhayma. Spark: Self-supervised personalized real-time monocular face capture. *arXiv preprint arXiv:2409.07984*, 2024. 2, 3
- [2] Yoshua Bengio, Aaron Courville, and P. Vincent. Representation learning: A review and new perspectives. *IEEE Transactions on Pattern Analysis and Machine Intelligence*, 35(8):1798–1828, Aug. 2013. 2
- [3] Timo Bolkart, Tianye Li, and Michael J. Black. Instant multi-view head capture through learnable registration. In *Conference on Computer Vision and Pattern Recognition (CVPR)*, pages 768–779, 2023. 4
- [4] Giorgos Bouritsas, Sergiy Bokhnyak, Stylianos Ploumpis, Michael Bronstein, and Stefanos Zafeiriou. Neural 3d morphable models: Spiral convolutional networks for 3d shape representation learning and generation. In *Proceedings of the IEEE/CVF international conference on computer vision*, pages 7213–7222, 2019. 4
- [5] Chen Cao, Yanlin Weng, Shun Zhou, Yiyong Tong, and Kun Zhou. Facewarehouse: A 3d facial expression database for visual computing. *IEEE Transactions on Visualization and Computer Graphics*, 20(3):413–425, 2013. 4
- [6] Marc-André Carbonneau, Julian Zaïdi, Jonathan Boilard, and Ghyslain Gagnon. Measuring disentanglement: A review of metrics. *IEEE Transactions on Neural Networks and Learning Systems*, 35(7):8747–8761, 2024. 2
- [7] Zenghao Chai, Haoxian Zhang, Jing Ren, Di Kang, Zhengzhuo Xu, Xuefei Zhe, Chun Yuan, and Linchao Bao. Realy: Rethinking the evaluation of 3d face reconstruction. In *European conference on computer vision*, pages 74–92. Springer, 2022. 2, 3, 6, 12
- [8] Zenghao Chai, Tianke Zhang, Tianyu He, Xu Tan, Tadas Baltrusaitis, HsiangTao Wu, Runnan Li, Sheng Zhao, Chun Yuan, and Jiang Bian. Hiface: High-fidelity 3d face reconstruction by learning static and dynamic details. In *Proceedings of the IEEE/CVF International Conference on Computer Vision*, pages 9087–9098, 2023. 2, 8
- [9] Prashanth Chandran, Gaspard Zoss, Markus Gross, Paulo Gotardo, and Derek Bradley. Facial animation with disentangled identity and motion using transformers. In *Computer Graphics Forum*, volume 41, pages 267–277. Wiley Online Library, 2022. 3
- [10] Radek Daněček, Michael J Black, and Timo Bolkart. Emoca: Emotion driven monocular face capture and animation. In *Proceedings of the IEEE/CVF Conference on Computer Vision and Pattern Recognition*, pages 20311–20322, 2022. 2, 3, 7
- [11] Radek Daněček, Kiran Chhatre, Shashank Tripathi, Yandong Wen, Michael Black, and Timo Bolkart. Emotional speech-driven animation with content-emotion disentanglement. In *SIGGRAPH Asia 2023 Conference Papers*, SA '23, New York, NY, USA, 2023. Association for Computing Machinery. 2, 3, 7, 8, 9
- [12] Paul Debevec. The light stages and their applications to photoreal digital actors. *SIGGRAPH Asia*, 2(4):1–6, 2012. 1
- [13] Yu Deng, Jiaolong Yang, Sicheng Xu, Dong Chen, Yunde Jia, and Xin Tong. Accurate 3d face reconstruction with weakly-supervised learning: From single image to image set. In *Proceedings of the IEEE/CVF conference on computer vision and pattern recognition workshops*, pages 0–0, 2019. 2
- [14] Abdallah Dib, Luiz Gustavo Hafemann, Emeline Got, Trevor Anderson, Amin Fadaeinejad, Rafael MO Cruz, and Marc-André Carbonneau. Mosar: Monocular semi-supervised model for avatar reconstruction using differentiable shading. In *Proceedings of the IEEE/CVF Conference on Computer Vision and Pattern Recognition*, pages 1770–1780, 2024. 3, 4, 8
- [15] Nikita Drobyshev, Jenya Chelishev, Taras Khakhulin, Aleksei Ivakhnenko, Victor Lempitsky, and Egor Zakharov. Megaportraits: One-shot megapixel neural head avatars. In *Proceedings of the 30th ACM International Conference on Multimedia*, pages 2663–2671, 2022. 3, 6
- [16] Bernhard Egger, William AP Smith, Ayush Tewari, Stefanie Wuhler, Michael Zollhoefer, Thabo Beeler, Florian Bernard, Timo Bolkart, Adam Kortylewski, Sami Romdhani, et al. 3d morphable face models-past, present, and future. *ACM Transactions on Graphics (TOG)*, 39(5):1–38, 2020. 2
- [17] Yao Feng, Haiwen Feng, Michael J Black, and Timo Bolkart. Learning an animatable detailed 3d face model from in-the-wild images. *ACM Transactions on Graphics (ToG)*, 40(4):1–13, 2021. 2, 3, 8
- [18] Yao Feng, Haiwen Feng, Michael J. Black, and Timo Bolkart. Learning an animatable detailed 3d face model from in-the-wild images. *ACM Trans. Graph.*, 40(4), July 2021. 7, 9
- [19] David Ferman, Pablo Garrido, and Gaurav Bharaj. Facelift: Semi-supervised 3d facial landmark localization. In *Proceedings of the IEEE/CVF Conference on Computer Vision and Pattern Recognition (CVPR)*, pages 1781–1791, June 2024. 7
- [20] Panagiotis P Filntisis, George Retsinas, Foivos Paraperas-Papantoniou, Athanasios Katsamanis, Anastasios Roussos, and Petros Maragos. Spectre: Visual speech-informed perceptual 3d facial expression reconstruction from videos. In *Proceedings of the IEEE/CVF Conference on Computer Vision and Pattern Recognition*, pages 5745–5755, 2023. 2, 3
- [21] Blender Foundation. Cycles renderer. <https://www.cycles-renderer.org/>, 2021. Accessed: 2024-11-07. 5
- [22] Yaroslav Ganin and Victor Lempitsky. Unsupervised domain adaptation by backpropagation. In *International conference on machine learning*, pages 1180–1189. PMLR, 2015. 5

- [23] Simon Giebenhain, Tobias Kirschstein, Markos Georgopoulos, Martin Rünz, Lourdes Agapito, and Matthias Nießner. Learning neural parametric head models. In *Proc. IEEE Conf. on Computer Vision and Pattern Recognition (CVPR)*, 2023. 3
- [24] Kaiming He, Xiangyu Zhang, Shaoqing Ren, and Jian Sun. Identity mappings in deep residual networks. In *Computer Vision–ECCV 2016: 14th European Conference, Amsterdam, The Netherlands, October 11–14, 2016, Proceedings, Part IV 14*, pages 630–645. Springer, 2016. 5
- [25] Charlie Hewitt, Fatemeh Saleh, Sadegh Aliakbarian, Lohit Petikam, Shideh Rezaeifar, Louis Florentin, Zafairah Hoseinie, Thomas J Cashman, Julien Valentin, Darren Cosker, et al. Look ma, no markers: holistic performance capture without the hassle. *arXiv preprint arXiv:2410.11520*, 2024. 3
- [26] Gee-Sern Hsu, Chun-Hung Tsai, and Hung-Yi Wu. Dual-generator face reenactment. In *Proceedings of the IEEE/CVF conference on computer vision and pattern recognition*, pages 642–650, 2022. 6
- [27] Dongjin Huang, Yongsheng Shi, Jinhua Liu, and Wen Tang. Self-supervised learning for fine-grained monocular 3d face reconstruction in the wild. *Multimedia Systems*, 30(4):235, 2024. 2
- [28] IEEE. *A 3D Face Model for Pose and Illumination Invariant Face Recognition*, Genova, Italy, 2009. 2, 8
- [29] Hiroharu Kato, Deniz Beker, Mihai Morariu, Takahiro Ando, Toru Matsuoka, Wadim Kehl, and Adrien Gaidon. Differentiable rendering: A survey. *arXiv preprint arXiv:2006.12057*, 2020. 2, 3
- [30] Diederik Kingma and Jimmy Ba. Adam: A method for stochastic optimization. In *International Conference on Learning Representations (ICLR)*, San Diego, CA, USA, 2015. 5, 7
- [31] Biwen Lei, Jianqiang Ren, Mengyang Feng, Miaomiao Cui, and Xuansong Xie. A hierarchical representation network for accurate and detailed face reconstruction from in-the-wild images. In *Proceedings of the IEEE/CVF Conference on Computer Vision and Pattern Recognition*, pages 394–403, 2023. 2
- [32] Ruilong Li, Karl Bladin, Yajie Zhao, Chinmay Chinara, Owen Ingraham, Pengda Xiang, Xinglei Ren, Pratusha Prasad, Bipin Kishore, Jun Xing, et al. Learning formation of physically-based face attributes. In *Proceedings of the IEEE/CVF conference on computer vision and pattern recognition*, pages 3410–3419, 2020. 2, 8
- [33] Tianye Li, Timo Bolkart, Michael J. Black, Hao Li, and Javier Romero. Learning a model of facial shape and expression from 4D scans. *ACM Transactions on Graphics, (Proc. SIGGRAPH Asia)*, 36(6):194:1–194:17, 2017. 2, 6
- [34] Zhuang Liu, Hanzi Mao, Chao-Yuan Wu, Christoph Feichtenhofer, Trevor Darrell, and Saining Xie. A convnet for the 2020s. In *Proceedings of the IEEE/CVF conference on computer vision and pattern recognition*, pages 11976–11986, 2022. 5
- [35] Francesco Locatello, Stefan Bauer, Mario Lucic, Gunnar Raetsch, Sylvain Gelly, Bernhard Schölkopf, and Olivier Bachem. Challenging common assumptions in the unsupervised learning of disentangled representations. In *International Conference on Machine Learning*, 2019. 2
- [36] Francesco Locatello, Michael Tschannen, Stefan Bauer, Gunnar Rätsch, Bernhard Schölkopf, and Olivier Bachem. Disentangling factors of variations using few labels. In *International Conference on Learning Representations*, 2020. 2
- [37] Anurag Ranjan, Timo Bolkart, Soubhik Sanyal, and Michael J. Black. Generating 3D faces using convolutional mesh autoencoders. In *European Conference on Computer Vision (ECCV)*, pages 725–741, 2018. 4
- [38] Qiuyu Ren, Zhiying Lu, Haopeng Wu, Jianfeng Zhang, and Zijian Dong. Hr-net: a landmark based high realistic face reenactment network. *IEEE Transactions on Circuits and Systems for Video Technology*, 33(11):6347–6359, 2023. 6
- [39] George Retsinas, Panagiotis P Filntisis, Radek Danecsek, Victoria F Abrevaya, Anastasios Roussos, Timo Bolkart, and Petros Maragos. 3d facial expressions through analysis-by-neural-synthesis. In *Proceedings of the IEEE/CVF Conference on Computer Vision and Pattern Recognition*, pages 2490–2501, 2024. 2, 3, 7, 8, 9
- [40] Mostafa Sadeghi, Xavier Alameda-Pineda, and Radu Horaud. Unsupervised performance analysis of 3d face alignment with a statistically robust confidence test. *Neurocomputing*, 564:126941, 2024. 2
- [41] Soubhik Sanyal, Timo Bolkart, Haiwen Feng, and Michael Black. Learning to regress 3D face shape and expression from an image without 3D supervision. In *Proceedings IEEE Conf. on Computer Vision and Pattern Recognition (CVPR)*, pages 7763–7772, June 2019. 2, 3
- [42] Bernhard Schölkopf, Dominik Janzing, Jonas Peters, Eleni Sgouritsa, Kun Zhang, and Joris Mooij. On causal and anticausal learning. In *International Conference on Machine Learning*, 2012. 2
- [43] Ayush Tewari, Ohad Fried, Justus Thies, Vincent Sitzmann, Stephen Lombardi, Kalyan Sunkavalli, Ricardo Martin-Brualla, Tomas Simon, Jason Saragih, Matthias Nießner, et al. State of the art on neural rendering. In *Computer Graphics Forum*, volume 39, pages 701–727. Wiley Online Library, 2020. 3
- [44] Daniel Vlasic, Matthew Brand, Hanspeter Pfister, and Jovan Popovic. Face transfer with multilinear models. In *ACM SIGGRAPH 2006 Courses*, pages 24–es. 2006. 3
- [45] Zidu Wang, Xiangyu Zhu, Tianshuo Zhang, Baiqin Wang, and Zhen Lei. 3d face reconstruction with the geometric guidance of facial part segmentation. In *Proceedings of the IEEE/CVF Conference on Computer Vision and Pattern Recognition*, pages 1672–1682, 2024. 2, 3, 8, 9
- [46] Erroll Wood, Tadas Baltrušaitis, Charlie Hewitt, Sebastian Dziadzio, Thomas J Cashman, and Jamie Shotton. Fake it till you make it: face analysis in the wild using synthetic data alone. In *Proceedings of the IEEE/CVF international conference on computer vision*, pages 3681–3691, 2021. 2, 3, 5, 14
- [47] Erroll Wood, Tadas Baltrušaitis, Charlie Hewitt, Matthew Johnson, Jingjing Shen, Nikola Milosavljević, Daniel Wilde,

- Stephan Garbin, Toby Sharp, Ivan Stojiljković, et al. 3d face reconstruction with dense landmarks. In *European Conference on Computer Vision*, pages 160–177. Springer, 2022. 2
- [48] Erroll Wood, Tadas Baltrušaitis, Charlie Hewitt, Matthew Johnson, Jingjing Shen, Nikola Milosavljević, Daniel Wilde, Stephan Garbin, Toby Sharp, Ivan Stojiljković, et al. 3d face reconstruction with dense landmarks. In *European Conference on Computer Vision*, pages 160–177. Springer, 2022. 3
- [49] Wayne Wu, Chen Qian, Shuo Yang, Quan Wang, Yici Cai, and Qiang Zhou. Look at boundary: A boundary-aware face alignment algorithm. In *Proceedings of the IEEE conference on computer vision and pattern recognition*, pages 2129–2138, 2018. 6
- [50] Yuxin Wu and Kaiming He. Group normalization. In *Proceedings of the European conference on computer vision (ECCV)*, pages 3–19, 2018. 5
- [51] Cheng-hsin Wu, Ningyuan Zheng, Scott Ardisson, Rohan Bali, Danielle Belko, Eric Brockmeyer, Lucas Evans, Timothy Godisart, Hyowon Ha, Xuhua Huang, Alexander Hypes, Taylor Koska, Steven Krenn, Stephen Lombardi, Xiaomin Luo, Kevyn McPhail, Laura Millerschoen, Michal Perdoch, Mark Pitts, Alexander Richard, Jason Saragih, Junko Saragih, Takaaki Shiratori, Tomas Simon, Matt Stewart, Autumn Trimble, Xinshuo Weng, David Whitewolf, Chenglei Wu, Shouo-I Yu, and Yaser Sheikh. Multiface: A dataset for neural face rendering. In *arXiv*, 2022. 2, 4, 6, 9, 12
- [52] Sicheng Xu, Guojun Chen, Yu-Xiao Guo, Jiaolong Yang, Chong Li, Zhenyu Zang, Yizhong Zhang, Xin Tong, and Baining Guo. Vasa-1: Lifelike audio-driven talking faces generated in real time. *arXiv preprint arXiv:2404.10667*, 2024. 3
- [53] Haotian Yang, Hao Zhu, Yanru Wang, Mingkai Huang, Qiu Shen, Ruigang Yang, and Xun Cao. Facescape: a large-scale high quality 3d face dataset and detailed riggable 3d face prediction. In *Proceedings of the IEEE/CVF conference on computer vision and pattern recognition*, pages 601–610, 2020. 3
- [54] Qingcheng Zhao, Pengyu Long, Qixuan Zhang, Dafei Qin, Han Liang, Longwen Zhang, Yingliang Zhang, Jingyi Yu, and Lan Xu. Media2face: Co-speech facial animation generation with multi-modality guidance. In *ACM SIGGRAPH 2024 Conference Papers*, pages 1–13, 2024. 3
- [55] Tinghui Zhou, Philipp Krähenbühl, Mathieu Aubry, Qixing Huang, and Alexei A. Efros. Learning dense correspondence via 3d-guided cycle consistency. In *2016 IEEE Conference on Computer Vision and Pattern Recognition (CVPR)*, pages 117–126, 2016. 4
- [56] Zhenglin Zhou, Huaxia Li, Hong Liu, Nanyang Wang, Gang Yu, and Rongrong Ji. Star loss: Reducing semantic ambiguity in facial landmark detection. In *Proceedings of the IEEE/CVF conference on computer vision and pattern recognition*, pages 15475–15484, 2023. 7
- [57] Hao Zhu, Wayne Wu, Wentao Zhu, Liming Jiang, Siwei Tang, Li Zhang, Ziwei Liu, and Chen Change Loy. Celebv-hq: A large-scale video facial attributes dataset. In *European conference on computer vision*, pages 650–667. Springer, 2022. 6
- [58] Wojciech Zielonka, Timo Bolkart, and Justus Thies. Towards metrical reconstruction of human faces. In *European conference on computer vision*, pages 250–269. Springer, 2022. 2, 3, 4

A. Appendices

A.1. Implementation details

For training the semantic face expression model, we use the following importance weight in eq. 1 of the main manuscript. $\lambda_{rec} = 0.001$, $\lambda_{cycle} = 1.0$, $\lambda_{delta} = 0.01$, $\lambda_{edge} = 10000$ and $\lambda_{eyes} = 0.01$. Details for the model’s architecture are provided Tab. 4.

For the Face capture model, the following importance weight are used in eq. 2 of the main manuscript: $\lambda_{code} = 10$, $\lambda_{lmks} = 1$ and $\lambda_{domain} = 0.005$. For the gradient reversal, we use a scale factor equal to 1. Details for the model’s architecture are provided Tab. 5.

A.2. MultiREX additional details

We built the MultiREX benchmark from 8 identities from the MultiFace dataset [51]. We selected a single Range-of-Motion (ROM) sequence per identity, where the subjects perform a large variety of facial movements, including extreme expressions. For each ROM video, we consider 5 camera views, with the exception of identity ‘002914589’ which only includes 4 (due to a camera failure). In total, we use 39 distinct videos. The benchmark comprises 10k ground truth meshes and 49k images. We note that while the original Multiface dataset contains 13 identities, we did not consider 5 subjects that either: (i) did not contain the range-of-motion sequence, (ii) had a camera failure for the frontal video or (iii) had videos that cropped a large portion of the subject’s face.

Fig. 7 presents a frame for the different views used for evaluation, using the frame we manually selected for neutral representation of each individual. This is followed by the corresponding ground-truth mesh under the multi-face topology and finally by the wrapped equivalent under the FLAME topology. FLAME neutrals are obtained using commercial software (Wrap 3D³), by first aligning each multiface mesh to the FLAME basehead with a rigid alignment with manually selected keypoints around eyes, nose, and mouth, then wrapping the mesh for topology conversion.

The evaluation is inspired by the REALY benchmark [7]. Four masks are considered in the Multiface topology, as illustrated in Fig. 8. For a given mesh under evaluation, we first perform a rigid alignment of the evaluated regions from the ground truth to the generated mesh. For cheek and mouth, the rigid alignment is done with the combination of the mouth and cheek mask. After rigid alignment, we compute the mean vertex distance between the ground truth and the alignment mesh part.



Figure 7. The 5 camera views used in MultiREX (left-to-right), followed by the corresponding ground-truth mesh under the Multiface and FLAME topology. We show all 8 subjects in the benchmark.

A.3. More comparisons

A.3.1 Comparison on MultiREX benchmark

In this section, we show more visual comparison against state-of-the-art methods on the MultiREX benchmark. Results are reported in Fig. 9, Fig. 10 and Fig. 11 for different subjects under different viewing angles. Our method shows robustness against side view changes and preserves better the subject’s expression compared to other methods that generate less consistent expression over different views.

A.3.2 Comparison on in-the-wild images

Here, we show more qualitative results for in-the-wild re-targeting to other subjects and considering different source expressions. Our model is more faithful to the source expression in most scenarios while accounting for the face

³<https://faceform.com/>

Function	Details
E_{exp}	<ul style="list-style-type: none"> • SpiralConv (x5) $(3, 32) \rightarrow (32, 32) \rightarrow (32, 32) \rightarrow (32, 64) \rightarrow (64, 64)$ • Linear: <code>Linear(3392, 64)</code>
E_{id}	<ul style="list-style-type: none"> • SpiralConv (x5) $(3, 32) \rightarrow (32, 32) \rightarrow (32, 32) \rightarrow (32, 64) \rightarrow (64, 64)$ • Linear: <code>Linear(3392, 64)</code>
D_{mesh}	<ul style="list-style-type: none"> • Linear: <code>Linear(128, 3392)</code> • SpiralConv (x5) $(64, 64) \rightarrow (64, 32) \rightarrow (32, 32) \rightarrow (32, 32) \rightarrow (32, 3)$

Table 4. Model architecture for the semantic expression model.

Function	Details
E_{img}	<ul style="list-style-type: none"> • ConvNeXt-B()
H_{code}	<ul style="list-style-type: none"> • ResBlock (x3): <code>Linear(512, 512) → GELU → GroupNorm(32, 512)</code> • Linear: <code>Linear(512, 64)</code>
H_{lmks}	<ul style="list-style-type: none"> • Linear: <code>Linear(512, 128)</code>
C_{d}	<ul style="list-style-type: none"> • GradientReversal() • Linear: <code>Linear(512, 256) → GroupNorm(16, 256) → GELU</code> • ResBlock (x2): <code>Linear(256, 256) → GELU → GroupNorm(16, 256)</code> • Linear: <code>Linear(256, 1)</code>

Table 5. Model architecture for the face expression capture model.

morphology and through its semantic expression model.

A.4. Synthetic dataset

Fig. 13 shows samples from our synthetic dataset used to train our face capture model. Rendering is done using Blender, with the Cycles renderer. We use randomly se-

lected environment maps⁴. We use the same meshes and textures for teeth and eyes for all subjects. They are placed procedurally based on the vertex positions of the eyelids and jaw.

We emphasize that the generation of our synthetic

⁴<https://polyhaven.com>

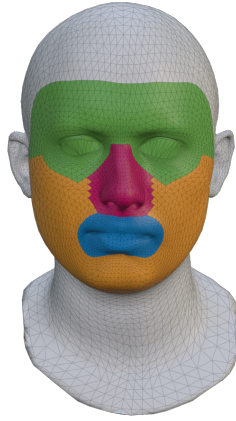


Figure 8. Visual representation of the forehead, nose, mouth, and cheek region masks used for our part-based evaluation. Masks do not overlap from one to another.

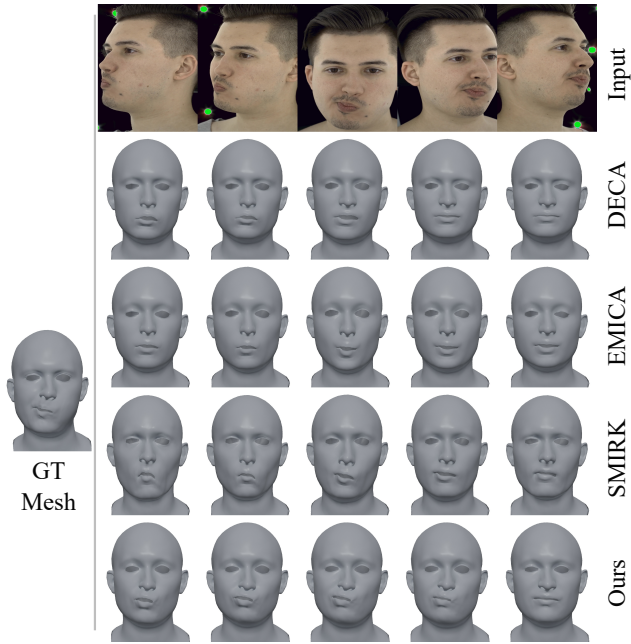


Figure 9. Additional captures on the proposed MultiREX benchmark

dataset does not require 3D modeling for hair, facial accessories, or clothes, contrary to [46].

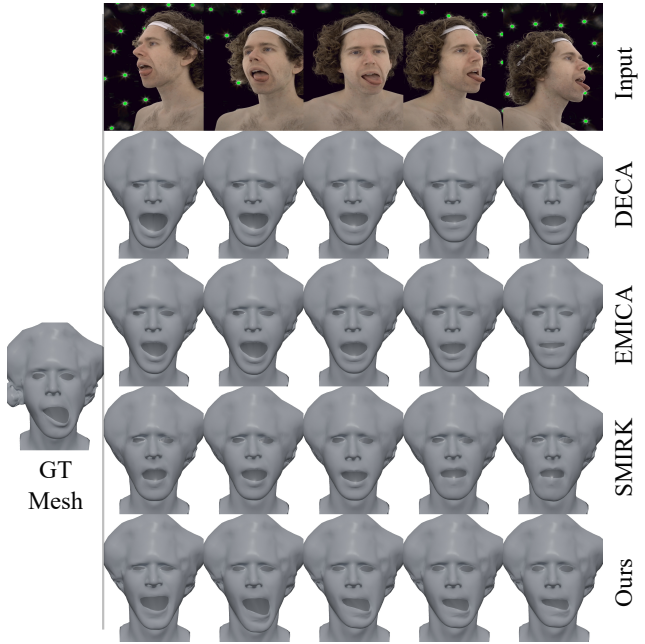


Figure 10. Additional captures on the proposed MultiREX benchmark

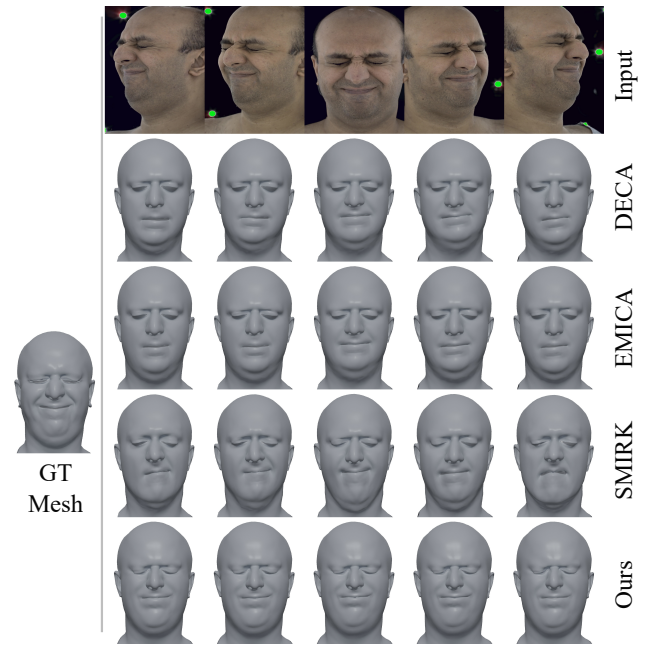


Figure 11. Additional captures on the proposed MultiREX benchmark

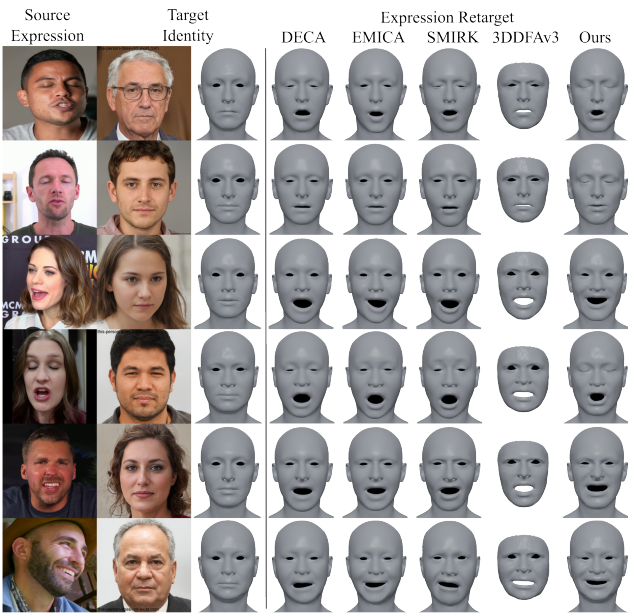


Figure 12. Additional retargeting on in-the-wild images

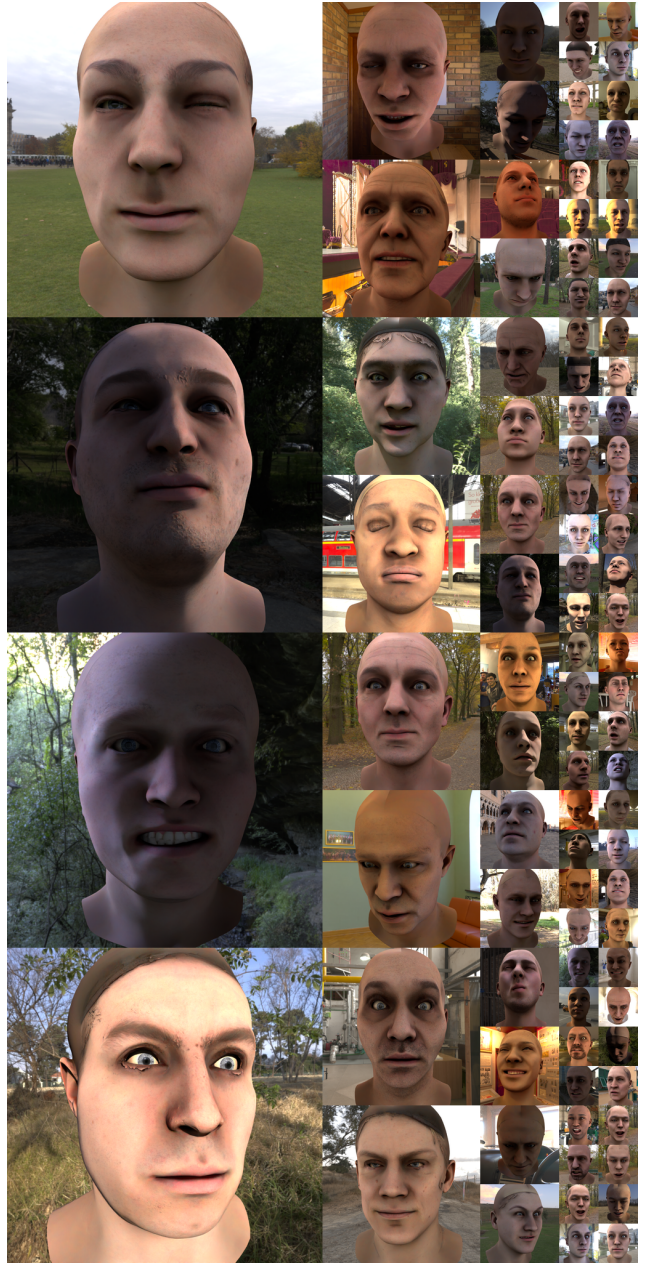


Figure 13. Random synthetic data samples.